frontiers | Frontiers in Materials

TYPE Original Research
PUBLISHED 25 May 2023
DOI 10.3389/fmats.2023.1179651

OPEN ACCESS

EDITED BY
Dhiren Kumar Pradhan,
The University of Tennessee, Knoxville, United States

REVIEWED BY
Shalini Kumari,
The Pennsylvania State University (PSU), United States
Tie Yang,
Southwest University, China

*CORRESPONDENCE
N. V. Ter-Oganessian,
teroganesyan@sfedu.ru
Kee Hoon Kim,
khkim@phya.snu.ac.kr

†PRESENT ADDRESS
Kee Hoon Kim, Seoul National University, Seoul, Republic of Korea

RECEIVED 04 March 2023
ACCEPTED 09 May 2023
PUBLISHED 25 May 2023

CITATION
Shahee A, Yoo K, Koteswararao B, Ter-Oganessian NV and Kim KH (2023), Observation of linear magnetoelectric effect in a Dirac magnon antiferromagnet Cu_3TeO_6. *Front. Mater.* 10:1179651. doi: 10.3389/fmats.2023.1179651

Observation of linear magnetoelectric effect in a Dirac magnon antiferromagnet Cu_3TeO_6

Aga Shahee[1,2], Kyongjun Yoo[1], B. Koteswararao[1,3], N. V. Ter-Oganessian[4]* and Kee Hoon Kim[1,5]*†

[1]Center for Novel States of Complex Materials Research, Department of Physics and Astronomy, Seoul National University, Seoul, Republic of Korea, [2]Centre for Interdisciplinary Research and Innovations, University of Kashmir, Srinagar, India, [3]Department of Physics, Indian Institute of Technology Tirupati, Tirupati, India, [4]Institute of Physics, Southern Federal University, Rostov-on-Don, Russia, [5]Department of Physics and Astronomy, Institute of Applied Physics, Seoul National University, Seoul, Republic of Korea

Cu_3TeO_6, a three-dimensional antiferromagnet forming a unique spin-web lattice of spin-1/2 Cu^{2+} ions below the Néel temperature $T_N \approx 62$ K, has recently been found to exhibit topological Dirac or nodal magnon dispersion. In this study, we report the discovery of the linear magnetoelectric (ME) effects in Cu_3TeO_6 below T_N. Our pyroelectric current measurements at a constant magnetic field (H) reveal a linear increase of electric polarization (P) with H for both $P//H$ and $P\perp H$ configurations; a maximum $P//[110] = 20\ \mu C/m^2$ is obtained at $\mu_0 H//[1\bar{1}0] = 14$ T, corresponding to a linear ME coefficient 1.8 ps/m. Magnetic point group analysis and Monte-Carlo simulations confirm that finite linear ME coefficients are allowed in the off-diagonal and diagonal ME tensor components, consistent with the magnetic point group of $\bar{3}'$. As the parity-time symmetry can be broken in the presence of H or electric field E in the linear ME materials, we envisage that Cu_3TeO_6 should exhibit a H- or E-induced transformation in the topological magnon dispersion from a Dirac point/nodal line type into two Weyl point types.

KEYWORDS

linear magnetoelectric effect, Dirac magnon, spin-induced ferroelectricity, Cu_3TeO_6, multiferroics and magnetoelectric coupling

Introduction

In the linear magnetoelectric (ME) materials, electric polarization (P) can be linearly induced by magnetic field (H) or magnetization (M) can be linearly induced by electric field (E). The linear ME effect was first discovered experimentally in an antiferromagnet Cr_2O_3 by Astrov (Astrov, 1960), after the theoretical predictions first by Landau and Lifshitz (Landau and Lifshitz, 1984) and later by Dzyaloshinskii (Dzyaloshinskii, 1959). The linear ME effect occurs when a material breaks space inversion (I) and time-reversal (t) symmetry separately but conserves the simultaneous operation of $I \otimes t$.

Since the first discovery, numerous linear ME materials have been discovered and studied, particularly in the 1960–1970s (O'Dell, 1970; Smolenskiĭ and Chupis, 1982). Furthermore, in the early 2000s, research interests on the ME effects were reignited by the discoveries of large non-linear ME effects in several multiferroic materials (Kimura et al, 2003; Wang et al, 2003; Hur et al, 2004). Over the last 2 decades, research on the multiferroics has been very active, leading to the discovery of numerous emergent multiferroics and new

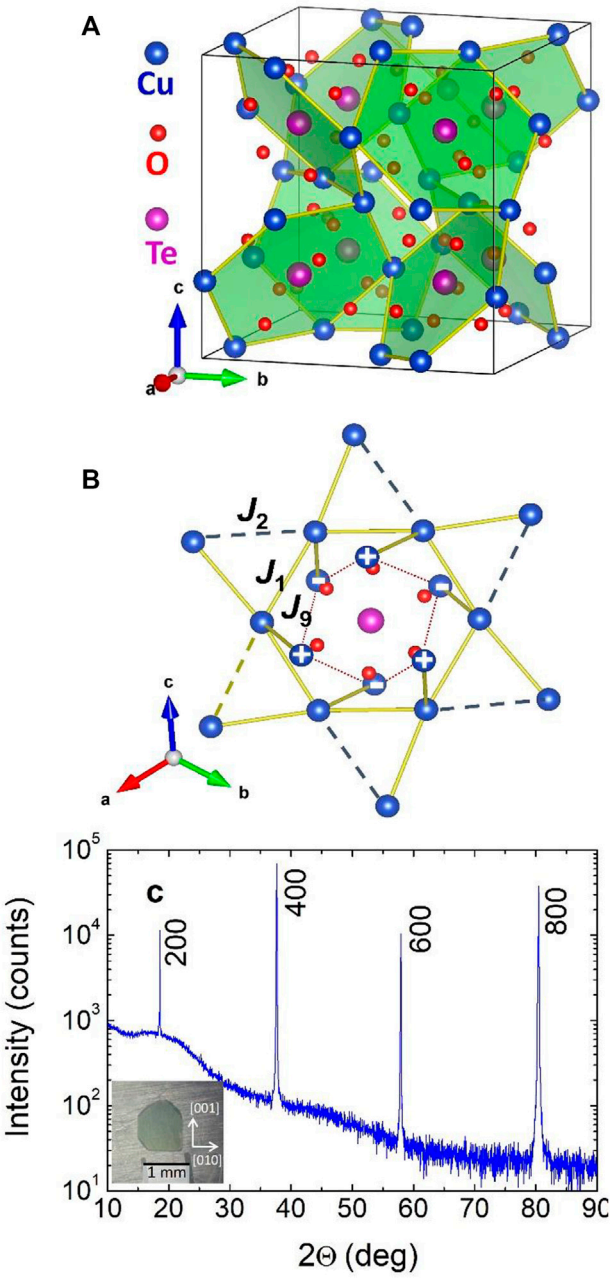

FIGURE 1
(A) The crystal structure of Cu_3TeO_6 including the eight Cu hexagons surrounding TeO_6 octahedra. **(B)** First (solid line), second (bold dash line), and nineth (weak dash line) nearest neighbor (NN) exchange interactions are drawn as J_1, J_2, and J_9, respectively. The plus (+) and minus (–) signs indicate Cu ions of neighbouring Cu hexagon at equal distance above and below the shown Cu hexagon of solid line and J_9 is exchange interactions between these two Cu ions. The 1st NN forms a hexagon and the 1st with the 2nd NN forms a hyper kagome structure. **(C)** XRD data taken along the [100] crystallographic direction with the inset picture of the Cu_3TeO_6 single crystal.

mechanisms for generating ME coupling (Cheong and Mostovoy, 2007; Spaldin and Ramesh, 2019). Very recently, even 2D van der Waals materials have been found to exhibit multiferroic behavior (Park et al, 2022). Moreover, a topologically protected switching mechanism has been recently identified in a multiferroic $GdMn_2O_5$ (Ponet et al, 2022). Additionally, while $BiFeO_3$ films have been studied for a long time, Shin et al, 2022 successfully grew high-quality thin films of Co_2Z hexaferrites exhibiting ME behavior at room temperature. Thus, scientific research on multiferroic and magnetoelectric materials seems to be still actively performed.

The ME materials possess unique properties that enable cross-coupling between magnetic and electrical properties, making them increasingly valuable for various next-generation electronic devices. Examples include highly sensitive *H* sensors with pico-tesla sensitivity (Zhai et al, 2006) and low-power non-volatile memories (Bibes and Barthélémy, 2008). Moreover, ME and/or multiferroic materials can be utilized as tunable filters, antennas, and resonators in millimetre-wave devices for wireless communication and radar (Li and Luk, 2016), ME logic circuits, which operate at a low voltage of ~100 mV, provide an energy-efficient alternative to traditional CMOS technology (Manipatruni et al, 2019), and flexible ME nanogenerators for energy harvesting (Ghosh et al, 2020). Thus, recent research has demonstrated the potential of ME materials to offer promising alternatives to the conventional technologies, making them highly attractive for applications.

In addition to research efforts aimed at finding practical applications for ME materials, studying the ME effects in magnetic insulators can be useful for understanding their basic properties. For example, the ME tensor characteristics of a magnetic insulator can serve as an effective means of determining its magnetic point group when neutron scattering fails to determine magnetic symmetry unambiguously. Moreover, as found in this work, the ME effect can also be utilized to manipulate the topological magnon properties of a magnetic insulator.

Cu_3TeO_6 belongs to corundum related compounds of A_3TeO_6 (*A* = Mn, Co, Ni, and Cu) family, which has recently attracted scientific attention due to its each members unique properties. Although they nominally have the same chemical formula, each member of A_3TeO_6 family exhibits different structural and physical properties based on the type of ions at the *A*-site. Mn_3TeO_6, for instance, adopts a trigonal structure ($R\bar{3}$ space group) and exhibits a complex incommensurate magnetic structure with multiferroic properties (Zhao et al, 2015; Ivanov et al, 2017), while Co_3TeO_6 crystallizes in a monoclinic structure (*C*2/*c* space group) and exhibits *H*-induced electric polarization (*P*) (Hudl et al, 2011; Leo et al, 2018). Moreover, Ni_3TeO_6 has a trigonal structure (*R*3 polar space group) and exhibits *P* in the spin-flop phase induced by *H* above 8 T (T) (Oh et al, 2014; Kim et al, 2015). On the other hand, Cu_3TeO_6 is known to crystalize in a cubic lattice structure of high symmetry ($Ia\bar{3}$ centrosymmetric space group) without any report on its electrical properties. It forms a unique bixbyite-type structure, in which 24 Cu^{2+}, 8 Te^{6+}, and 48 O^{2-} ions are contained in a unit cell, forming a network of 8 hexagons composed of 6 Cu^{2+} ions and a central Te^{6+} ion (See, Figure 1A). (Falck et al, 1978; Herak et al, 2005)

Upon the temperature being lowered, Cu_3TeO_6 undergoes a paramagnetic to an antiferromagnetic (AFM) spin ordering at the Néel temperature (T_N) of 62 K. This leads to the stabilization of a unique three-dimensional spin-web lattice of Cu^{2+} ions with $S = ½$ spins (Herak et al, 2005; Herak, 2011; Månsson et al, 2012; He and Itoh, 2014). An earlier report based on neutron powder diffraction and torque magnetometry measurements suggest the appearance of either a collinear AFM order or a slightly canted AFM order with the

dominant spin moment along one of [±1 ± 1±1] directions (Herak et al, 2005), forming a trigonal symmetry in the spin system (Herak et al, 2005). Recent theoretical predictions by Li *et al* (Li et al, 2017) suggest the existence of Dirac and the nodal line magnons for the collinear and spin canted state of Cu_3TeO_6, respectively. This was subsequently confirmed by Bao et al. (2018) and Yao et al. (2018), who reported the spin excitation spectra of Cu_3TeO_6 from the inelastic neutron scattering (INS) measurements. These experiments provided experimental evidence for the novel topological Dirac/nodal line magnons. However, the resolution of the magnon spectra from those two experiments was not sufficient to distinguish possible nodal lines from the Dirac point.

According to the theoretical prediction using the first-principles calculations and a linear-response theory by Wang et al, 2019, the Dirac point (or the Nodal line) in the magnon dispersion is coined to the absence (or presence) of a spin canting in the AFM state. The spin canting in Cu_3TeO_6 is most likely induced by the Dzyaloshinskii-Moriya interactions (DMI). These topological Dirac point and nodal line in the magnon dispersion suggest that $I \otimes t$ symmetry is preserved without any biased E and H, thus allowing the linear ME effect consistent with a magnetic point group. However, applied H and E for the ME poling may lead to the eventual stabilization of one type of ME domain and emergence of the transversal electric polarization. This would imply that the $I \otimes t$ symmetry is broken by the application of H or E. In this case, the magnon bands are expected to carry non-zero Berry curvature/Chern numbers, which may transfrom each Dirac point/nodal line into two Weyl points with opposite charges (Owerre, 2018). Therefore, investigating the ME effects in Cu_3TeO_6 can further our understanding of characteristic magnon dispersion at zero and finite H or E.

In this letter, we report the discovery of both off-diagonal and diagonal linear ME coupling in Cu_3TeO_6 below T_N = 62 K. Our findings indicates that the electric polarization ($P//[110]$) exhibits a linear increase under a magnetic field ($H//[1\bar{1}0]$) up to 14 T with the configuration of $P \perp H$. We conducted a combined symmetry analysis and Monte-Carlo calculations to confirm that the observed linear ME effect with both off-diagonal and diagonal components can be attributed to the magnetic point group $\bar{3}'$.

Results and discussions

Magnetic and electrical properties

The lattice structure of Cu_3TeO_6 and the arrangement of its magnetic ions (Cu^{2+}) are shown in Figures 1A,B, respectively. Cu_3TeO_6 crystalizes in a bixbyite-type high-symmetric cubic structure ($Ia\bar{3}$ space group) with 12 Cu^{2+} (S = ½) ions per primitive cell and with a lattice parameter of a = 9.537 Å at room temperature (Falck et al, 1978). Despite its simple structure, Cu_3TeO_6 exhibits a spin-web type antiferromagnetic ordering with topological magnon dispersion. The spin-lattice is composed of nearly coplanar hexagons formed by six Cu^{2+} (S = ½) ions with normal along the [±1 ± 1±1] directions. There are four different orientations of hexagons with normal along [111], [11–1], [1–11], or [–111], and each Cu^{2+} ion is shared by two hexagons, forming an unusual hyper kagome network (see, Figure 1B). A nearly straight Cu-O-O-Cu path can be observed between the 9th nearest neighbors. Recent INS (Yao et al, 2018) measurements and first-principles calculations (Wang et al, 2019) have shown that the strength of the 9th nearest-neighbour exchange interaction, which is antiferromagnetic, is comparable to the first nearest neighbor interaction, while the second and other nearest-neighbour exchange interactions are rather weak.

X-ray diffraction (XRD) data measured in the Cu_3TeO_6 single crystal with {100} plane are shown in Figure 1A. The data confirm that the Cu_3TeO_6 single crystal was grown without chemical impurities. Since the Cu_3TeO_6 has a cubic structure, the crystals have a clear rectangular shape with a size of ~1 mm^3, as seen in the inset of Figure 1C; Figure 2A displays the magnetic susceptibility (χ) data measured at H = 1 kOe along the cubic directions [100], [110], and [111] after zero-field cooling. The χ curves exhibit a downturn at T_N = 62 K along all directions, indicating the onset of a long-range AFM ordering below T_N. The χ curves are similar for each direction but show a minimum value along the [111] direction. (Herak et al, 2005; He and Itoh, 2014), suggesting that the [111] direction is the easy axis, although the magnetic anisotropy is quite weak. These results are consistent with earlier neutron scattering data (Herak et al, 2005), that suggest the spins are oriented parallel to the [111] axis in the AFM phase and the magnetic anisotropy is quite weak. This behavior is also qualitatively consistent with magnetic data reported by other groups (Caimi et al, 2006; Choi et al, 2008; Månsson et al, 2012; He and Itoh, 2014).

The Curie-Weiss fit of the inverse χ (Figure 2B) shows the Curie-Weiss temperature θ_{CW} = −160 K, whose absolute value is much higher than T_N. This θ_{CW} = −160 K is consistent with previously reported values ranging from −134 K to −213 K (Herak et al, 2005; Månsson et al, 2012; Bao et al, 2018; Yao et al, 2018) and indicates that the magnetic interactions are predominantly AFM. The value of the frustration index ($f = |\theta_{CW}|/T_N$) of 2.58 in our case and 2.23–3.55 in other previous reports suggests that the Cu_3TeO_6 is moderately frustrated (Herak et al, 2005; Månsson et al, 2012; Bao et al, 2018; Yao et al, 2018). It has been reported that except for the strong first "J_1," & ninth "J_9" and the moderate second "J_2," fourth "J_4," & 10th "J_{10}" exchange interactions, all other exchange interactions up to J_{20} are rather weak. The strong J_1 and J_9 are compatible with the collinear AFM ground state, while the modest frustration possibly comes from the incompatibility of the sizeable J_2, J_4, and J_{10} exchange interactions with the collinear AFM state (Wang et al, 2019). Besides, it is further found that χ starts to deviate from the Curie-Weiss law below −126 K possibly indicates the onset of short-range spin order (Yao et al, 2018).

We also measured the H-dependent magnetization (M) along three crystallographic directions ([100], [110] & [111]) at 5 K (Figures 2C,D). The M-H curve along the [111] direction shows a slight curve between −1.5 T and 1.5 T, whereas it is almost linear for the [100] and [110] directions (Herak et al, 2005). This change in the slope of the M-H curve along the [111] direction is due to the presence of four types of domains, each with the spins oriented along one of the body diagonal [111], [11–1], [1–11], or [–111] directions of the cubic unit cell, which then yield their H -induced rotation and alignment (Herak et al, 2005). The magnetization M increases almost linearly up to −0.086 μ_B/f.u at 9 T, which is still much lower than the expected saturation value of M_s = 3 μ_B/f.u. This confirms that the AFM spin configuration is maintained at least up to 9 T.

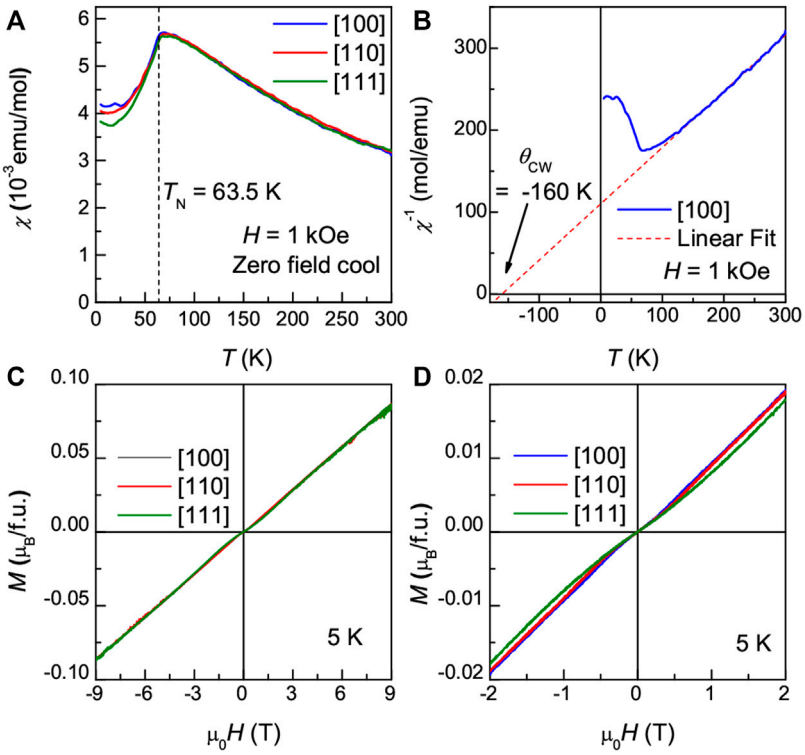

FIGURE 2
Temperature and magnetic dependence of magnetic properties of Cu_3TeO_6. **(A)** Magnetic susceptibility and **(B)** inverse susceptibility as a function of temperature and **(C, D)** magnetic field dependence of magnetization with two field ranges along each direction in the Cu_3TeO_6 single crystals.

To investigate ME coupling in Cu_3TeO_6, we measured the pyroelectric currents (I_p) and dielectric constant ε at selected H in a transverse configuration, i.e., I_p and ε//[110] and H//[1–10], as summarized in Figures 3A–D. Without the application of H, no observable I_p is measured, as shown in Figure 3A. However, upon application of H = 3 T, I_p at low temperature starts to decrease linearly above 20 K and shows a sharp dip near T_N = 62 K. As H increases beyond 3 T, the linear decrease and dip feature in I_p are progressively enhanced up to a maximum applicable field of H = 14 T, implying that P is continually enhanced with increasing H. The sign of I_p was reversed by a negative electric poling ($-E_P$) (data not shown here), which indicates that P is intrinsically induced by the broken inversion symmetry under H.

Figure 3B summarizes the temperature-dependence of the P obtained by integrating the I_p with time. For all applied H, P is nearly constant below 20 K, decreases above 20 K approximately as $\sqrt{T_N - T}$, and finally drops to zero at T_N. The reported temperature dependence of the staggered moment obtained from the neutron diffraction measurement (Herak et al, 2005) is similar to that of the $P(T)$ curves. This implies that the evolution of the magnetic order parameter in Cu_3TeO_6 below T_N is directly coupled to the evolution of P under H. These results provide further evidence of the strong ME coupling in Cu_3TeO_6.

In Figure 3C, we summarize the resultant P value at 2 K at each constant H. The figure shows that the p-value increases nearly linear with H until it reaches the maximum value of 20 $\mu C/m^2$ at $\mu_0 H$ = 14 T, which supports the linear ME coupling. We obtained linear ME coefficient α of 1.8 ps/m, which is lower than those observed in other important linear ME compounds such as $TbPO_4$ (730 ps/m, 1.5 K) (Rivera, 2009), and $LiCoPO_4$ (30.6 ps/m, 4.2 K) (Rivera and Schmid, 1994). However, the α value of ~1.8 ps/m is higher than those of $BiFeO_3$ (0.3 ps/m, 300 K), $GaFeO_3$ (0.06 ps/m, 300 K) (Niu et al, 2017), $(NH_4)_2$ [$FeCl_5$·(H_2O)] (1.2 ps/m, 1.5 K) (Hughey et al, 2022), and $LiNiPO_4$ (1.7 ps/m, 20 K) (Vaknin et al, 2004) although it is comparable to those of Cr_2O_3 (2.8 ps/m, 300 K) (Iyama and Kimura, 2013), $NdCrTiO_5$ (−1.84 ps/m, 10 K) (Li et al, 2018) and Sm_2BaCuO_5 (4.4 ps/m, 2 K) (Yanda et al, 2019). The relatively small ME effect of Cu_3TeO_6 might be due to the isotropic nature of S = ½ spins and the small spin-orbit coupling. It's worth noting that this linear ME effect is quite unique in the Cu^{2+} (S = 1/2) systems since most of the linear ME effect have been discovered in large spin (S > 1/2) systems with magnetic ions such as Cr, Fe, Mn, and Ni. Recently, in the family of Cu^{2+} (S = ½) system, we observed H-induced ferroelectricity in a kagome staircase compound $PbCu_3TeO_7$, whose origin is related to the type II multiferroicity coming from a spiral spin structure (Yoo et al, 2018).

Figures 3D,E summarizes the temperature dependence of the dielectric permittivity ε for E//[110] at several magnetic fields (i.e. 0, 3, 6, 9, 12 & 14 T) applied along the H//[1–10] direction. At zero H, ε exhibits a weak drop at T_N = 62 K. When H = 3 T is applied, there is a sharp jump of ε at T_N and the magnitude of this jump increases greatly with increasing H. It is worth noting that ε at 2 K increases tremendously from 13.4 at 0 T to 29.8 at 14 T. Moreover, the dielectric loss also shows a large change under H (not shown

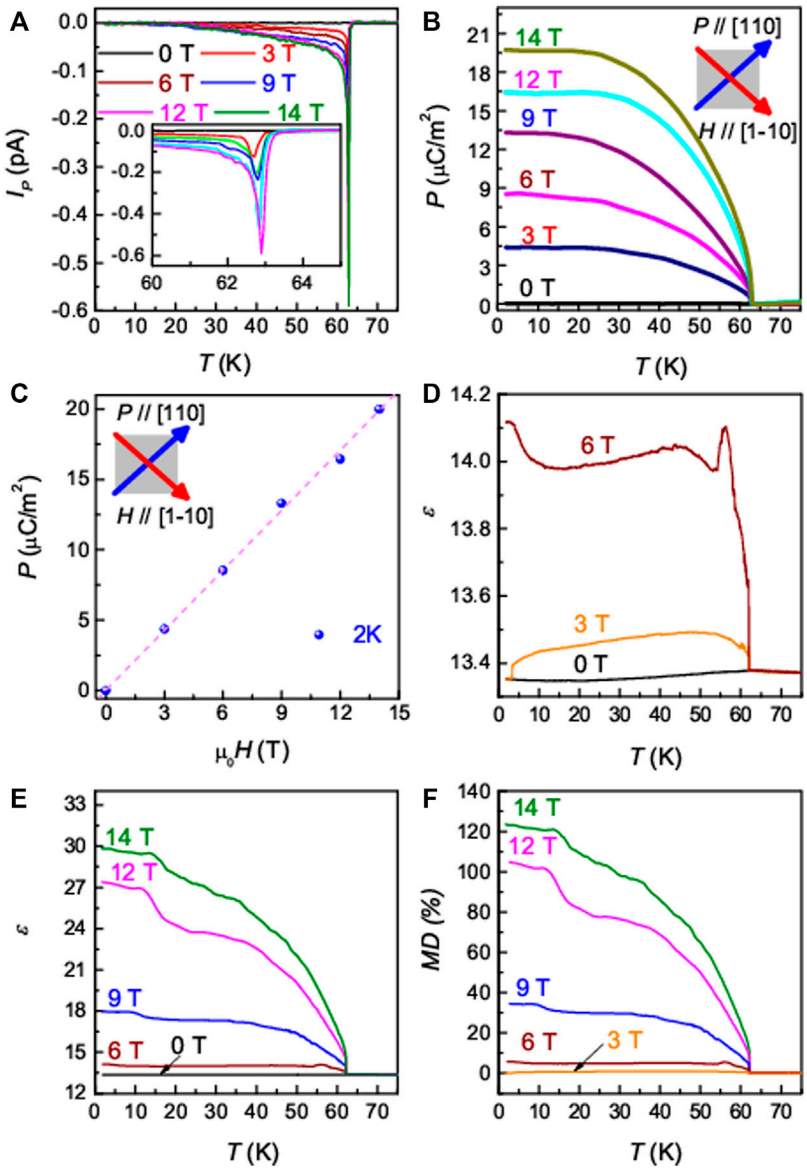

FIGURE 3
Temperature dependence of electric properties of Cu_3TeO_6. The **(A)** pyroelectric current along [110] for *E*//[110] at various *H*//[1–10], **(B)** the electric polarization *P*//[110] at various *H*//[1–10], **(C)** summarizes the electric polarization *P*//[110] at various *H*//[1–10] at 2 K **(D, E)** the dielectric constant for *P*,*E*//[110] and *H*//[1–10] and **(F)** the corresponding magnetodielectric (MD) effect in Cu_3TeO_6 single crystals.

here). The magneto-dielectric (MD) effect, calculated using the formula, $\text{MD}\ (H) = \frac{\varepsilon'(H)-\varepsilon'(0)}{\varepsilon'(0)} \times 100\%$, is summarized in Figure 3F as a function of T at different H. This shows that Cu_3TeO_6 exhibits a positive, giant MD response below T_N with maximum MD of 123% at 2 K at H = 14 T. The observation of the giant MD effect in Cu_3TeO_6 directly reflects the presence of large modulations in the lattice degrees of freedom under an applied H, thereby supporting the intrinsic nature of the magnetoelectric effect.

To investigate the possibility of a ME response induced by H in other crystallographic directions and configurations, we conducted measurements of the I_p curves in different H and P directions. The P curves obtained by integrating the I_p data over time are presented in Figure 4. These P curves show that the polarization for all configurations emerges at T_N, at which ε exhibits an anomaly for all the investigated configurations. Further, the $P(T)$ curves show the same line shapes but different values for different directions. At 2 K and 9 T, P values for the (*P*//[110], *H*//[1–10]), (*P*//[110], *H*//[110]), (*P*//[100], *H*//[010]), and (*P*//[100], *H*//[100]) configurations are 13.3 μC/m², 1.4 μC/m², 7.4 μC/m², and 0.8 μC/m², respectively. These observations indicate that the emergence of P with H in this linear ME system is not restricted to only one highly symmetric lattice direction. Among them, the maximum ME coefficient of 1.8 ps/m is realized in the direction of *P*//[110] with *H*//[1–10]. It is worth noting that P is an order of magnitude larger in the $H \perp P$ configurations than in the $H//P$ configurations, indicating that the off-diagonal components of the linear ME tensor are dominant.

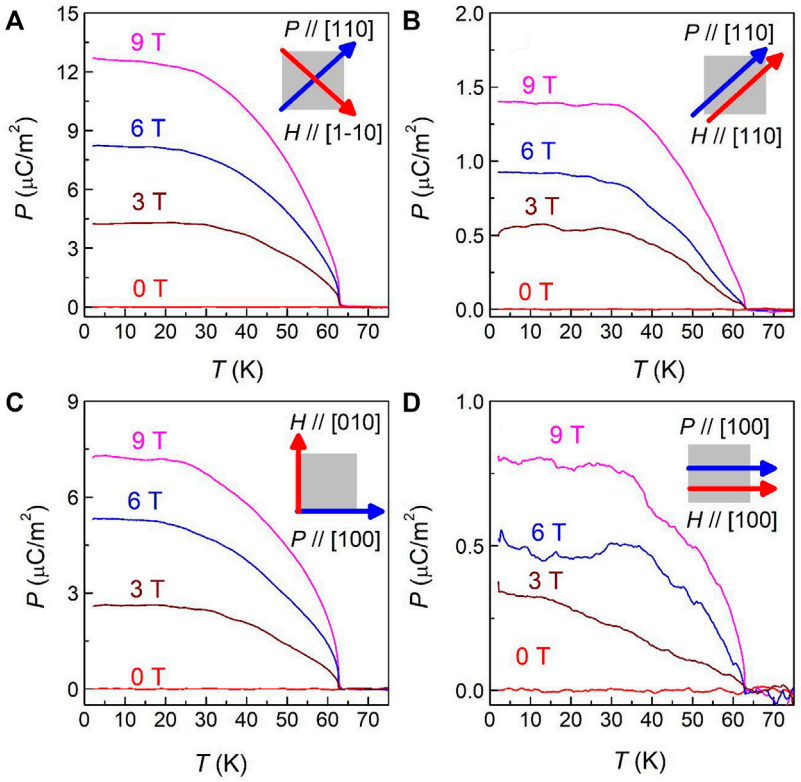

FIGURE 4
Temperature dependence of electric polarization of Cu_3TeO_6 single crystals measured for various directions of P and H directions, as represented by schematic inset figures for each dataset. The data were collected at various H and presented for **(A)** P//[110] with H//[1-10], **(B)** P//[110] with H//[110], **(C)** P//[100] with H//[010] and **(D)** P//[100] with H//[100]. The transverse configurations exhibit a significantly large P, providing evidence for the presence of dominant off-diagonal ME tensors in Cu_3TeO_6.

These experimental results thus reveal that a particular form of the linear ME tensor associated with a specific magnetic point group should be responsible for the induced P at a finite H below T_N.

The symmetry analysis and the classical Monte-Carlo simulations

Next, we would like to discuss the possible mechanism of ME coupling in Cu_3TeO_6. For that, we performed symmetry analysis and conducted classical Monte-Carlo simulations using the exchange constants available from the literature data (Yao et al, 2018; Wang et al, 2019). According to the neutron diffraction data (Herak et al, 2005), the magnetic structure appearing below T_N is described by the wavevector $\vec{k} = 0$. The magnetic representation Γ_m for the 12 magnetic Cu^{2+} ions in the primitive cell is split into

$$\Gamma_m = \Gamma^{1+} \oplus \Gamma^{1-} \oplus \Gamma^{2+3+} \oplus \Gamma^{2-3-} \oplus 5\Gamma^{4+} \oplus 5\Gamma^{4-},$$

where Γ^{2+3+} and Γ^{2-3-} are physically irreducible representations (IR). The AFM ordering observed by the neutron diffraction experiment is described by IR Γ^{4-}, which enters five times into Γ_m and according to which five order parameters are transformed. Three of these order parameters (a_1, a_2, a_3), (b_1, b_2, b_3), and (c_1, c_2, c_3) describe the collinear magnetic structure. The phase state of the form (a, a, a) with all three order parameters being equal gives the direction of spins along the [111] direction. The proposed noncollinearity is described either by the remaining two order parameters transforming according to IR Γ^{4-}, which are necessarily condensed at the Γ^{4-} instability at T_N, or by the order parameter q described by IR Γ^{1-}, which is induced by Γ^{4-} in an improper way due to the interaction

$$a_1 a_2 a_3 q.$$

The magnetoelectric interactions that result in H-induced electric polarization below T_N are

$$I_1 = a_1 M_y P_z + a_2 M_z P_x + a_3 M_x P_y, \quad (1)$$
$$I_2 = a_1 M_z P_y + a_2 M_x P_z + a_3 M_y P_x, \quad (2)$$

where any of the five order parameters transformed according to Γ^{4-} can replace (a_1, a_2, a_3). As mentioned above, the magnetic structure belongs to the phase state (a, a, a), which has eight domains (the spins can be oriented predominantly along one of the four spatial diagonals of the cubic cell). Magnetoelectric poling prior to the measurements partially lifts this degeneracy.

For the analysis of the ME behavior one can write the expansion of the thermodynamic potential as a function of the order parameters in the form

$$\Phi = \Phi_0 + \kappa_1 (I_1 - I_2) + \kappa_2 (I_1 + I_2) - \vec{M}\vec{H} - \vec{P}\vec{E}$$
$$= \Phi_0 + \kappa_1 \left[a_1\left(M_y P_z - M_z P_y\right) + a_2 (M_z P_x - M_x P_z)\right.$$
$$\left. + a_3\left(M_x P_y - M_y P_x\right)\right] + \kappa_2 \left[a_1\left(M_y P_z + M_z P_y\right) + a_2 (M_z P_x + M_x P_z)\right.$$
$$\left. + a_3\left(M_x P_y + M_y P_x\right)\right] - \vec{M}\vec{H} - \vec{P}\vec{E}, \quad (3)$$

with

$$\Phi_0 = \frac{A}{2}\left(a_1^2 + a_2^2 + a_3^2\right) + \frac{B_1}{4}\left(a_1^4 + a_2^4 + a_3^4\right) + \frac{B_2}{4}\left(a_1^2 + a_2^2 + a_3^2\right)^2$$
$$+ \frac{1}{2\varepsilon}\left(P_x^2 + P_y^2 + P_z^2\right) + \frac{1}{2\chi}\left(M_x^2 + M_y^2 + M_z^2\right),$$

where A, B_1, and B_2 are phenomenological coefficients, and ε and χ are dielectric and magnetic susceptibilities, respectively.

According to our results, the H-induced polarization for the P//[110] and H//[1–10] geometry is much larger than for P//[110] and H//[110]. In the former case, the ME coefficient is κ_1, while in the latter, it is κ_2. This indicates that κ_1 is much larger than κ_2. In the case of P//[100] and H//[010], the ME coefficient is $\kappa_1 - \kappa_2$ and, therefore, should be close to the case of P//[110] and H//[1–10]. However, for the former case (i.e., the case of P//[100] and H//[010] in Figure 4C, the H-induced polarization is about as twice lower than for the latter case (i.e., the case of P//[110] and H//[1–10] in Figure 4A. In our view, this larger than-expected difference is the result of higher order ME interactions with respect to the AFM order parameter. Indeed, there are many additional third-order ME interactions in the AF order parameter, which are linear with respect to magnetization and electric polarization, e.g.,

$$a_1 a_2 a_3\left(M_x P_x + M_y P_y + M_z P_z\right).$$

From our point of view, such interactions are responsible for the electric polarization induced by H in the P//[100] and H//[100] geometry, for which interactions (1) and (2) give 0 ME effect.

To gain further insights into the microscopic interactions, we rewrote the magnetoelectric interactions (1) and (2) in terms of the spins of the ions in the primitive cell, and we analyzed and discussed the resulting numerous microscopic interactions in the Supporting Material.

Implications of the ME effects on the topological magnon dispersion

Although Cu_3TeO_6 with a centrosymmetric $Ia\bar{3}$ space group possesses a global center of inversion, Cu-O-Cu bond angles smaller than 180° lead to the breaking of the local inversion symmetry around the region where a ligand ion lies between two magnetic ions. The absence of this local inversion symmetry allows in principle the DMI leading to spin canting. According to the neutron diffraction study of Herak *et al* (Herak et al, 2005), the AFM ordering of Cu_3TeO_6 below $T_N = 62$ K leads to either collinear or slightly tilted non-collinear spin configuration with a dominant magnetic moment along one of the [±1 ± 1±1] directions. This concomitantly results in a decrease in crystal symmetry from cubic to trigonal.

According to theoretical calculations by Li *et al* (Li et al, 2017), who refer to the experimental spin canting angles of 6° within the spin pair connected by the strongest interaction J_1, the value of $|D_1|/|J_1|$ in Cu_3TeO_6 was estimated as ~ 0.2. However, Wang *et al* (Wang et al, 2019) has considered all the J_i (i = 1–20) superexchange interactions, in which J_9 is the second strongest one, and estimated $|D_1|/|J_1|$ ~0.06 in Cu_3TeO_6, resulting in only the spin canting angle of only ~1.3° between the J_1 pair. Moreover, in this case, the value of $|D_9|$ corresponding to the second strongest J_9 was found to be negligible, because the bond angle corresponding to this exchange coupling (i.e., J_9) is very close to 180°. As a result, Wang *et al* (Wang et al, 2019) have predicted that the length of the nodal line should be proportional to $[|D_i|/|J_i|]^2$. However, the expected length of the nodal line is indeed very short so that it is difficult to differentiate the nodal line from the Dirac point according to the available INS data (Bao et al, 2018; Yao et al, 2018).

According to the theoretical calculations of Li et al. (2017) and Wang et al. (2019) the Dirac point and the Nodal line in the magnon dispersion are coined to the absence and the presence of a spin canting in the AFM state of Cu_3TeO_6, respectively. However, from our point of view, the prediction of nodal lines in Cu_3TeO_6 is the consequence of the simplicity of the model with only two exchange interactions (Li et al, 2017). Indeed, experimental INS results suggest the absence of nodal lines, and an involvement of many exchange paths, which is also supported by theoretical calculations (Bao et al, 2018; Yao et al, 2018). The INS experiment, however, indicates possible presence of Dirac points in the Γ and P points of the Brillouin zone, which should be allowed if the conservation of $I \otimes t$ -symmetry is valid.

Below T_N, the linear ME effect causes the electric and magnetic fields to have the same symmetry in Cu_3TeO_6. As a result, applying either field in Cu_3TeO_6 will break the remaining $I \otimes t$ symmetry, leading to either the transformation of Dirac points into the Weyl points or the appearance of energy gaps. The extent of the splitting or gap formation will be proportional to the applied field strength. Since magnons are neutral without any orbital effect and do not change quasi-momentum under external fields, the Weyl points will persist even under strong fields. Therefore, the magnon spectra in Cu_3TeO_6 can be manipulated by both H and electric field via a Zeeman coupling and the ME coupling, respectively. We expect both magnetic and electric fields to be equally effective in manipulating the topological magnon structure, but experimental verification is required to confirm their effectiveness.

Conclusion

In conclusion, we observed a linear ME effect in Cu_3TeO_6 with a maximum value of P = 20 μC/m^2 at $\mu_0 H$ = 14 T and a corresponding linear ME coefficient α = 1.8 ps/m for the P//[110] and H//[1–10] configuration. Moreover, the ME coefficient is one order of magnitude higher for transversal configurations compared to parallel configurations. Detailed symmetry analysis indicates that the linear ME effect originates from the ME tensor components allowed by the magnetic point group $\bar{3}'$ symmetry. Thus, Cu_3TeO_6 is a rare material that exhibits both topological quantum spin excitations and linear magnetoelectricity, demonstrating the richness of its physics. We suggest that the manipulation of topological properties can be achieved by both applied electric and magnetic fields, leading to the transformation of Dirac points into Weyl points or the appearance of energy gaps. This work will pave the way for electric field control of

topological magnon dispersion in Cu_3TeO_6. Further research on neutron scattering under magnetic or electric fields, as well as theoretical simulation, will be useful in shedding more light on the intriguing possibility of manipulating topological magnon dispersion.

Experimental methods

Single crystals of Cu_3TeO_6 were grown by the flux method. First, a polycrystalline Cu_3TeO_6 powder was prepared using high purity CuO (>99.99%) and TeO_2 in molar ratio of 3:1 via the solid-state reaction method. The powder was calcined at 600°C for 12 h twice and sintered at 850°C for 24 h. Then single crystals were grown using a mixture of polycrystalline Cu_3TeO_6 and PbO/TeO_2 flux (a molar ratio 1:1) at a mass ratio of 1:2. The mixture was heated at 950°C for 12 h and then cooled to 700°C at a rate of 1.25°C/h. Single crystals, ~1 mm^3 size and cubic in shape, were mechanically separated from the flux. The lattice structure of the grown Cu_3TeO_6 single crystals was characterized using an X-ray diffractometer (Empyrian™, Malverin Pananalytycal).

To conduct electrical measurements, the single crystals were shaped into a thin plate form along the [100] and [110] directions, and electrodes were made with silver epoxy on both sides of the plate. Magnetic properties were investigated using a vibrating sample magnetometer (VSM). Pyroelectric current (I_p) and dielectric constant (ε) were measured using an electrometer (Keithley, KE617) and a capacitance bridge (Andeen-Hagerling, AH2550A), respectively. These measurements were performed in a temperature (T) range from 2 to 75 K using a PPMS™ (Quantum Design, 9 T) or a Janis cryostat equipped with a 14 T superconducting magnet (Cryogenic^{LTD}). Prior to I_p measurements, the sample was first cooled down from 70 to 2 K under applications of an electric field of 1.2 MV/m and magnetic fields of 0, 3, 9, 12, and 14 T. After cooling, the electric field was removed and both sides of the electrode were short-circuited until stray charges were fully nullified. The I_p at zero electric field was recorded during temperature-warming mode under applications of constant magnetic fields. Electric polarization (P) was obtained by integrating I_p over time. Furthermore, for all the configurations, it has been confirmed that the sign of the P is reversed by reversing the direction of a poling electric field.

Note added in submission

During the preparation of the manuscript, we became aware that the linear magnetoelectric effect in Cu_3TeO_6 has been similarly reported in a recent preprint by Kisiček et al, arXiv:2211.08902. However, in the preprint paper, only P along [100] direction was measured, while we carried out investigations along different crystallographic directions. Thus, the authors of arXiv: 2211.08902 have only found the off-diagonal components of ME tensor, in contrast to the results in this manuscript.

Data availability statement

The original contributions presented in the study are included in the article/Supplementary Material, further inquiries can be directed to the corresponding authors.

Author contributions

BK prepared the single-crystal samples. KY measured the magnetization and susceptibility in PPMS. KY performed the dielectric constant, pyrocurrent, and ME current measurements in a 14 T magnet. NT-O did the MC calculation. AS, KY, NT-O, and KK. analyzed the data and wrote the manuscript. KK. devised the project and advised the research. All authors contributed to the article and approved the submitted version.

Funding

This work was supported by the Ministry of Science and ICT through NRF of the National Research Foundation of South Korea funded by Ministry of Science and ICT (2019R1A2C2090648, 2022H1D3A3A01077468) and core facility program funded by the Ministry of Education (2021R1A6C101B418).

Acknowledgments

We acknowledge financial support from the Ministry of Science and ICT through NRF of the National Research Foundation of South Korea funded by Ministry of Science and ICT (2019R1A2C2090648, 2022H1D3A3A01077468) and core facility program funded by the Ministry of Education (2021R1A6C101B418) for supporting this work. NT-O acknowledges financial support by the Ministry of Science and Higher Education of the Russian Federation (State assignment in the field of scientific activity, Southern Federal University, 2023, Project No. FENW-2023-0015) and AS acknowledges financial support from the Department of Science and Technology in India through the Ramanujan Faculty Award (RJF/2021/000122/SSC). BK acknowledges the funding from Department of Science and Technology, India.

Conflict of interest

The authors declare that the research was conducted in the absence of any commercial or financial relationships that could be construed as a potential conflict of interest.

Publisher's note

Supplementary material

The Supplementary Material for this article can be found online at: https://www.frontiersin.org/articles/10.3389/fmats.2023.1179651/full#supplementary-material

References

Astrov, D. N. (1960). The magnetoelectric effect in antiferromagnetics. *J. Exp. Theor. Phys.* 38, 984–985. doi:10.1021/jp000114x

Bao, S., Wang, J., Wang, W., Cai, Z., Li, S., Ma, Z., et al. (2018). Discovery of coexisting Dirac and triply degenerate magnons in a three-dimensional antiferromagnet. *Nat. Commun.* 9, 2591. doi:10.1038/s41467-018-05054-2

Bibes, M., and Barthélémy, A. (2008). Towards a magnetoelectric memory. *Nat. Mater.* 7, 425–426. doi:10.1038/nmat2189

Caimi, G., Degiorgi, L., Berger, H., and Forró, L. (2006). Optical evidence for a magnetically driven structural transition in the spin web Cu3TeO6. *Europhys. Lett.* 75, 496–502. doi:10.1209/epl/i2005-10603-3

Cheong, S.-W., and Mostovoy, M. (2007). Multiferroics: A magnetic twist for ferroelectricity. *Nat. Mater* 6, 13–20. doi:10.1038/nmat1804

Choi, K. Y., Lemmens, P., Choi, E. S., and Berger, H. (2008). Lattice anomalies and magnetic excitations of the spin web compound $Cu^{3}TeO^{6}$. *J. Phys. Condens. Matter* 20, 505214. doi:10.1088/0953-8984/20/50/505214

Dzyaloshinskii, I. E. (1959). On the magnetoelectrical effect in antiferromagnetics. *J. Exp. Theor. Phys.* 37, 881–882.

Falck, L., Lindqvist, O., and Moret, J. (1978). Tricopper(II) tellurate(VI). *Acta Crystallogr. B* 34, 896–897. doi:10.1107/S0567740878004276

Ghosh, S. K., Roy, K., Mishra, H. K., Sahoo, M. R., Mahanty, B., Vishwakarma, P. N., et al. (2020). Rollable magnetoelectric energy harvester as a wireless IoT sensor. *ACS Sustain Chem. Eng.* 8, 864–873. doi:10.1021/acssuschemeng.9b05058

He, Z., and Itoh, M. (2014). Magnetic behaviors of Cu3TeO6 with multiple spin lattices. *J. Magn. Magn. Mater* 354, 146–150. doi:10.1016/j.jmmm.2013.11.009

Herak, M., Berger, H., Prester, M., Miljak, M., Živković, I., Milat, O., et al. (2005). Novel spin lattice in Cu3TeO6: An antiferromagnetic order and domain dynamics. *J. Phys. Condens. Matter* 17, 7667–7679. doi:10.1088/0953-8984/17/48/017

Herak, M. (2011). Cubic magnetic anisotropy of the antiferromagnetically ordered Cu3TeO6. *Solid State Commun.* 151, 1588–1592. doi:10.1016/j.ssc.2011.07.024

Hudl, M., Mathieu, R., Ivanov, S. A., Weil, M., Carolus, V., Lottermoser, Th., et al. (2011). Complex magnetism and magnetic-field-driven electrical polarization of Co3TeO6. *Phys. Rev. B* 84, 180404. doi:10.1103/PhysRevB.84.180404

Hughey, K. D., Lee, M., Nam, J., Clune, A. J., O'Neal, K. R., Tian, W., et al. (2022). High-field magnetoelectric and spin-phonon coupling in multiferroic (NH4)2 [FeCl5·(H 2O)]. *Inorg. Chem.* 61, 3434–3442. doi:10.1021/acs.inorgchem.1c03311

Hur, N., Park, S., Sharma, P. A., Ahn, J. S., Guha, S., and Cheong, S. W. (2004). Electric polarization reversal and memory in a multiferroic material induced by magnetic fields. *Nature* 429, 392–395. 2004. (6990 429), doi:10.1038/nature02572

Ivanov, S. A., Ritter, C., Nordblad, P., Tellgren, R., Weil, M., Carolus, V., et al. (2017). New insights into the multiferroic properties of Mn3TeO6. *J. Phys. D. Appl. Phys.* 50, 085001. doi:10.1088/1361-6463/aa5621

Iyama, A., and Kimura, T. (2013). Magnetoelectric hysteresis loops in Cr2O3 at room temperature. *Phys. Rev. B* 87, 180408. doi:10.1103/PhysRevB.87.180408

Kim, J. W., Artyukhin, S., Mun, E. D., Jaime, M., Harrison, N., Hansen, A., et al. (2015). Successive magnetic-field-induced transitions and colossal magnetoelectric effect in Ni3TeO6. *Phys. Rev. Lett.* 115, 137201. doi:10.1103/PhysRevLett.115.137201

Kimura, T., Goto, T., Shintani, H., Ishizaka, K., Arima, T., and Tokura, Y. (2003). Magnetic control of ferroelectric polarization. *Nature* 426, 55–58. 55 426. doi:10.1038/nature02018

Landau, L. D., and Lifshitz, E. M. (1984). "Ferromagnetism and antiferromagnetism," in *Electrodynamics of continuous media* (Amsterdam, Netherlands; Elsevier, 130–179.

Leo, N., Carolus, V., White, J. S., Kenzelmann, M., Hudl, M., Tolédano, P., et al. (2018). Magnetoelectric inversion of domain patterns. *Nature* 560, 466–470. doi:10.1038/s41586-018-0432-4

Li, K., Li, C., Hu, J., Li, Y., and Fang, C. (2017). Dirac and nodal line magnons in three-dimensional antiferromagnets. *Phys. Rev. Lett.* 119, 247202. doi:10.1103/PhysRevLett.119.247202

Li, X., Liu, M., Wang, Y., Tian, L., Shi, R., Yang, L., et al. (2018). Magnetoelectric mutual-control in collinear antiferromagnetic NdCrTiO5. *Appl. Phys. Lett.* 113, 122903. doi:10.1063/1.5047077

Li, Y., and Luk, K.-M. (2016). A multibeam end-fire magnetoelectric dipole antenna array for millimeter-wave applications. *IEEE Trans. Antennas Propag.* 64, 2894–2904. doi:10.1109/TAP.2016.2554601

Manipatruni, S., Nikonov, D. E., Lin, C., Gosavi, tanay A., Liu, H., Prasad, B., et al. (2019). Scalable energy-efficient magnetoelectric spin–orbit logic. *Nature* 565, 35–42. doi:10.1038/s41586-018-0770-2

Månsson, M., Prša, K., Sugiyama, J., Andreica, D., Luetkens, H., and Berger, H. (2012). Magnetic order and transitions in the spin-web compound Cu3TeO6. *Phys. Procedia* 30, 142–145. doi:10.1016/j.phpro.2012.04.059

Niu, H., Pitcher, M. J., Corkett, A. J., Ling, S., Mandal, P., Zanella, M., et al. (2017). Room temperature magnetically ordered polar corundum GaFeO3 displaying magnetoelectric coupling. *J. Am. Chem. Soc.* 139, 1520–1531. doi:10.1021/jacs.6b11128

O'Dell, T. H. T. (1970). *The electrodynamics of magneto-electric media*. North-Holland, Amsterdam: North-Holland.

Oh, Y. S., Artyukhin, S., Yang, J. J., Zapf, V., Kim, J. W., Vanderbilt, D., et al. (2014). Non-hysteretic colossal magnetoelectricity in a collinear antiferromagnet. *Nat. Commun.* 5, 3201. doi:10.1038/ncomms4201

Owerre, S. A. (2018). Floquet Weyl magnons in three-dimensional quantum magnets. *Sci. Rep.* 8, 10098. doi:10.1038/s41598-018-28508-5

Park, C. B., Shahee, A., Kim, K., Patil, D. R., Guda, S. A., Ter-Oganessian, N., et al. (2022). Observation of spin-induced ferroelectricity in a layered van der Waals antiferromagnet CuCrP2S6. *Adv. Electron Mater* 8, 2101072. doi:10.1002/aelm.202101072

Ponet, L., Artyukhin, S., Kain, T., Wettstein, J., Pimenov, A., Shuvaev, A., et al. (2022). Topologically protected magnetoelectric switching in a multiferroic. *Nature* 607, 81–85. 81 607. doi:10.1038/s41586-022-04851-6

Rivera, J.-P., and Schmid, H. (1994). Search for the piezomagnetoelectric effect in LiCoPO4. *Ferroelectrics* 161, 91–97. doi:10.1080/00150199408213357

Rivera, J. P. (2009). A short review of the magnetoelectric effect and related experimental techniques on single phase (multi-) ferroics. *Eur. Phys. J. B* 71, 299–313. 3 71. doi:10.1140/EPJB/E2009-00336-7

Shin, K. W., Soroka, M., Shahee, A., Kim, K. H., Buršík, J., Kužel, R., et al. (2022). Observation of anomalously large magnetoelectric coupling in the hexagonal Z-type ferrite films. *Adv. Electron Mater* 8, 2101294. doi:10.1002/aelm.202101294

Smolenskiĭ, G. A., and Chupis, I. E. (1982). *Ferroelectromagnets*. Sov. Phys. Uspekhi 25, 475–493. doi:10.1070/PU1982v025n07ABEH004570

Spaldin, N. A., and Ramesh, R. (2019). Advances in magnetoelectric multiferroics. *Nat. Mater.* 18, 203–212. 3 18. doi:10.1038/s41563-018-0275-2

Vaknin, D., Zarestky, J. L., Rivera, J.-P., and Schmid, H. (2004). Commensurate-incommensurate magnetic phase transition in magnetoelectric single crystal LiNiPO4. *Phys. Rev. Lett.* 92, 207201. doi:10.1103/PhysRevLett.92.207201

Wang, D., Bo, X., Tang, F., and Wan, X. (2019). Calculated magnetic exchange interactions in the Dirac magnon material Cu3TeO6. *Phys. Rev. B* 99, 035160. doi:10.1103/PhysRevB.99.035160

Wang, J., Neaton, J. B., Zheng, H., Nagarajan, V., Ogale, S. B., Liu, B., et al. (2003). Epitaxial BiFeO3 multiferroic thin film heterostructures. *Science* 299, 1719–1722. 1979. doi:10.1126/science.1080615

Yanda, P., Ter-Oganessian, N. V., and Sundaresan, A. (2019). Linear magnetoelectric effect in antiferromagnetic Sm2BaCuO5. *Phys. Rev. B* 100, 104417. doi:10.1103/PhysRevB.100.104417

Yao, W., Li, C., Wang, L., Xue, S., Dan, Y., Iida, K., et al. (2018). Topological spin excitations in a three-dimensional antiferromagnet. *Nat. Phys.* 14, 1011–1015. doi:10.1038/s41567-018-0213-x

Yoo, K., Koteswararao, B., Kang, J., Shahee, A., Nam, W., Balakirev, F. F., et al. (2018). Magnetic field-induced ferroelectricity in S = 1/2 kagome staircase compound PbCu3TeO7. *NPJ Quantum Mater* 3, 45. doi:10.1038/s41535-018-0117-0

Zhai, J., Xing, Z., Dong, S., Li, J., and Viehland, D. (2006). Detection of pico-Tesla magnetic fields using magneto-electric sensors at room temperature. *Appl. Phys. Lett.* 88, 062510. doi:10.1063/1.2172706

Zhao, L., Hu, Z., Kuo, C. Y., Pi, T. W., Wu, M. K., Tjeng, L. H., et al. (2015). Mn3TeO6 - a new multiferroic material with two magnetic substructures. *Phys. Status Solidi - Rapid Res. Lett.* 9, 730–734. doi:10.1002/pssr.201510347